Plasmon-controlled narrower and blue-shifted fluorescence emission in (Au@SiO2)SiC nanohybrids

Ning Sui, Virginie Monnier, Yuriy Zakharko, Yann Chevolot, Sergei Alekseev, Jean-Marie Bluet, Vladimir Lysenko, Eliane Souteyrand

J Nanopart Res (2012) 14:1004
DOI 10.1007/s11051-012-1004-4

RESEARCH PAPER

Plasmon-controlled narrower and blue-shifted fluorescence emission in (Au@SiO_2)SiC nanohybrids

Ning Sui · Virginie Monnier · Yuriy Zakharko · Yann Chevolot · Sergei Alekseev · Jean-Marie Bluet · Vladimir Lysenko · Eliane Souteyrand

Received: 13 March 2012 / Accepted: 15 June 2012

Abstract Fluorescent imaging is a key tool in biology. On one hand, organic dyes are subjected to bleaching; while, on the other hand II–VI semiconductor quantum dots are photostable, but may exhibit some toxicity. Silicon carbide nanoparticles (SiC NPs) are a good alternative as SiC is chemically inert and considered as biocompatible material. However, their fluorescence quantum yield is weak. Plasmon-controlled fluorescence appears as a mean to enhance SiC NPs fluorescence. To this aim, new fluorescent nanohybrids (NHs) involving a gold colloid surrounded by a silica shell and overcoated with SiC NPs have been engineered. Au@SiO_2 particles were synthesized via a sol–gel method to obtain a controlled thickness of silica around gold colloid. Then, SiC NPs were immobilized onto silica by covalent bonding. TEM was used to study the structural properties of NHs. The influence of several parameters on NHs' fluorescence properties was investigated. It reveals that excitation wavelength must be chosen as close as possible to the gold plasmon band to avoid quenching of emission due to energy transfer between gold absorption and SiC emission. Moreover, the silica thickness is a key parameter to obtain high enhancement; for gold colloids of 20 nm in diameter overcoated by a 25 nm shell, an enhancement factor as high as 12.5 was obtained with a narrower and blue-shifted emission band. This blue-shift can be attributed to the surface chemistry modification of SiC NPs when they are covalently bonded to silica.

Keywords Core–shell nanoparticles · Plasmon · Fluorescence · Enhancement · Silicon carbide

Electronic supplementary material The online version of this article (doi:10.1007/s11051-012-1004-4) contains supplementary material, which is available to authorized users.

N. Sui · V. Monnier (✉) · Y. Chevolot · E. Souteyrand
Université de Lyon, Institut des Nanotechnologies de Lyon-INL, UMR CNRS 5270, Site Ecole Centrale de Lyon, 36 Avenue Guy de Collongue, 69134 Ecully, Cedex, France
e-mail: virginie.monnier@ec-lyon.fr

Y. Zakharko · J.-M. Bluet · V. Lysenko
Université de Lyon, Institut des Nanotechnologies de Lyon-INL-UMR 5270-CNRS, Site INSA Lyon, 7 Avenue Jean Capelle, 69621 Villeurbanne, Cedex, France

S. Alekseev
Faculty of Chemistry, Kiev National Taras Schevchenko University, 64 Vladimirskaya Str., 01601 Kiev, Ukraine

Introduction

Silicon carbide (SiC) is known to be a biocompatible and chemically inert material (Mélinon et al. 2007). Recently, SiC nanoparticles (NPs) were used successfully without any further functionalization for the fluorescent imaging of mouse conjunctiva fibroblast (Botsoa et al. 2008) and human fetal osteoblast cells (Fan et al. 2008). These NPs exhibit a fluorescence quantum yield of 17 % (Fan et al. 2008), which is quite low when compared to some efficient organic dyes like

Published online: 04 July 2012

fluorescein (97 %) or Texas Red (93 %) and CdSe quantum dots (65–85 %) (Resch-Genger et al. 2008). Thus, they should be injected into cells at a relatively high concentration (0.1 g L^{-1}) to obtain a clear labeling effect (Botsoa 2008). However, MTT (3-(4,5-dimethylthiazol-2-yl)-2,5-diphenyltetrazolium bromide) assays have evidenced that a significant decrease of cell proliferation is detected from 0.05 g L^{-1} SiC NPs concentration (Botsoa 2008). Therefore, even if they are chemically inert, the accumulation of NPs leads to undesirable physiological changes, which is not acceptable for a marker that should not be seen by the cells. Another disadvantage of SiC is its very broad emission band (due to large size distribution) ranging from 500 to 800 nm, which makes spectral multiplexing experiments impossible. Thus, to be competitive with usual fluorophores, the fluorescence intensity of SiC NPs must be enhanced ideally with a narrower emission band.

Plasmon-controlled fluorescence (PCF) (Lakowicz 2006) appears when a metal is located close to a fluorescent emitter. The oscillating electrons due to plasmon can become resonant with an incident light radiation. This can induce very strong and localized electromagnetic fields, which are able to enhance significantly the number of radiative processes of the fluorescent emitters. In particular, the coupling between plasmonic modes and fluorescent emitters is linked to several interesting properties: an amplification of the fluorescence signal, a better photostability, an enhancement of fluorescence quantum yield, and a better localization with low-intensity wide-field illumination (Lakowicz 2001; Lakowicz 2006).

In this work, we have elaborated new fluorescent-plasmonic nanohybrids (NHs) to enhance the fluorescence signal of SiC NPs (Fig. 1). These NHs are constituted by a gold core overcoated with a silica shell, followed by the addition of SiC NPs onto the surface of silica. Silica was chosen as the spacer material between Au and SiC for several reasons: (i) SiO_2 is a chemically inert material that could prevent aggregation, (ii) the thickness of SiO_2 coating can be controlled easily by sol–gel synthesis, and (iii) SiO_2 is an optically transparent and dielectric medium, where plasmon scattering can be achieved up to few hundreds of nanometers. A similar approach was already used by several groups using either organic dyes such as oxazine 725 (Ming et al. 2009) or carboxyfluorescein (Tovmachenko et al. 2006), inorganic quantum dots such as CdSe (Liu et al. 2006) or CdTe/CdS (Zheng et al. 2010), and rare-earth doped oxide nanoparticles (Y_2O_3:Er) (Zhang et al. 2010) as fluorescent emitters. The originality of our approach is to combine only chemically inert materials to elaborate a potential "all-biocompatible" nanoprobe. Moreover, with their weak quantum yield (17 %), SiC NPs are good candidates for fluorescence enhancement. Indeed, it has been shown that the expected enhancement can be as large as the inverse of the intrinsic quantum yield (Lakowicz 2001). Thus, the most interesting enhancement is obtained for low intrinsic quantum yield fluorescent emitters.

In this paper, we have elaborated (Au@SiO_2)SiC NHs where SiC NPs were covalently immobilized onto silica surface. Our aim was to obtain stable NHs with optimized fluorescence enhancement. The influence of silica shell thickness and excitation wavelength was studied.

Experimental

Chemicals

Gold colloids (diameter: 20 nm, ~0.01 % $HAuCl_4$), tetraethyl orthosilicate (TEOS), 3-aminopropyltrimethoxysilane (APTMS), sodium silicate solution ($Na_2O(SiO_2)_{3-5}$, 27 wt% SiO_2), ethanol, and ammonia solution (25–28 %) were purchased from Sigma-Aldrich. *N*,*N*′-diisopropylcarbodiimide (DIC) and *N*-hydroxysuccinimide (NHS) were obtained from Fluka. Milli-Q water (18.2 MΩ) was used in all the preparations.

Synthesis of Au@SiO_2 particles

The synthesis of Au@SiO_2 particles was achieved following a reported procedure with some modifications (Liz-Marzán et al. 1996). In a typical synthesis, a freshly prepared aqueous solution of APTMS (14.5 μL, 1 mM) was added into 5 mL of Au colloids dispersion under vigorous magnetic stirring. After keeping the mixture stand for 15 min, a 0.54 wt% sodium silicate solution (200 μL) was added to this solution, which was stirred for an additional 24 h. Gold particles with a thin silica shell (~2 nm) can be collected by centrifugation (960×*g* during 1 h). Then, these particles were transferred into 6 mL of a 1:5 water/ethanol mixture; to this, 125 μL of ammonia solution and TEOS are added. The volume of TEOS

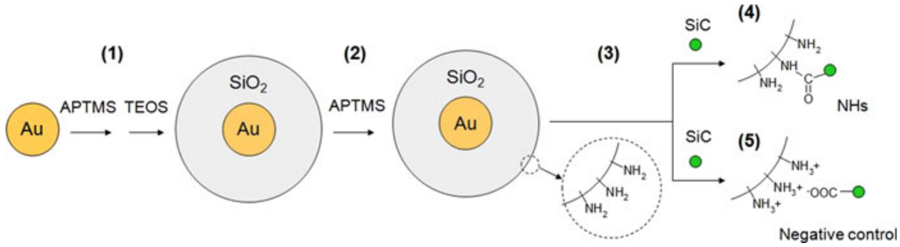

Fig. 1 Multistep synthesis of $(Au@SiO_2)SiC$ NHs. (*1*) $Au@SiO_2$ particles are synthesized by a two-step process: (i) surface modification of gold colloids by APTMS, (ii) silica shell growth by addition of TEOS. (*2*) $Au@SiO_2$ particles are modified by APTMS to obtain amino-functionalized silica surface. (*3*) Chemical bonding is achieved between amino groups and carboxylic groups from SiC NPs. NHs are elaborated via the formation of a covalent amide bond (*4*) while the spontaneously formed electrostatic bond serves as negative control for SiC NPs immobilization (*5*)

was set to 2.5, 6, and 20 μL to obtain 25, 40, and 80 nm silica thicknesses, respectively. The solution was allowed for reacting overnight under mild magnetic stirring. The product was separated by centrifugation at 10,600×*g* for 10 min and finally dispersed in 5 mL of ethanol.

Preparation and size selection of SiC NPs

SiC NPs were prepared by a previously reported method based on electrochemical etching (Botsoa et al. 2008). The obtained SiC nanopowder was dispersed in water and then centrifuged at 4,900×*g* for 3 min to sediment large crystallites at the bottom of the centrifugation tube and to collect the useful top part of the suspension containing only less polydisperse NPs with a diameter ranging between 1 and 3 nm. These NPs are highly stable in water. Finally, the concentration of SiC dispersion was set to 1 g L^{-1}.

Surface functionalization of $Au@SiO_2$ particles with amino groups

$Au@SiO_2$ particles were functionalized with APTMS by a reported method (VanBlaaderen and Vrij 1993). The amount of APTMS was calculated to be sufficient to provide approximately a 5-monolayer coating on silica particles (Westcott et al. 1998). 50 μL of APTMS solution in ethanol (1 mM) was added into 1 mL of $Au@SiO_2$ dispersion (7×10^{11} particles/mL). After stirring overnight, the dispersion was refluxed at 80 °C for an additional 2 h. The APTMS-functionalized $Au@SiO_2$ particles were purified by several centrifugation-washing steps with ethanol at 10,600×*g*. The surface density of amino groups was determined by Brilliant Coomassie Blue titration (Coussot et al. 2009) as described in the supporting information.

Preparation of $(Au@SiO_2)SiC$ NHs

After an ester activation of SiC surface carboxylic groups, SiC NPs were covalently immobilized onto amino-functionalized $Au@SiO_2$ particles through amide bond formation (Fig. 1). A 1 g L^{-1} dispersion of SiC NPs in water was used. The amount added to $Au@SiO_2$ particles was evaluated by two ways. For $Au@SiO_2$ particles with a 25-nm silica shell, the calculated volume necessary to cover silica with one monolayer of SiC NPs (mean diameter ~1.5 nm) was evaluated to be 6.9 μL. The calculation was also performed using absorbance measurements of the supernatant during SiC immobilization onto silica. In this case, the experimental value was 4 μL. The difference between theoretical and experimental calculation is because covering the silica surface with one compact monolayer of SiC is impossible due to electrostatic repulsion between SiC NPs. Thus, to insure that all SiC NPs will be immobilized and that no multilayer of SiC will be formed, the volume of SiC NPs dispersion to be added was fixed below these two values, i e., at 3 μL.

To achieve the covalent immobilization, 200 μL of $Au@SiO_2-NH_2$ particle dispersion (containing 1.4×10^{11} particles) was mixed with 3 μL of SiC NP dispersion (1 g L^{-1}) in water. Then, the mixture was dried under vacuum. Dry tetrahydrofuran containing NHs and DIC (molar ratio of NHS/DIC = 1:2.5) were added subsequently. The mixture was refluxed at 60 °C in dry tetrahydrofuran for 4 h. The NHs were purified by centrifugation and the precipitate was dispersed in a 1:1 water/ethanol mixture for characterization.

As a negative control, Au@SiO_2 particles with electrostatically immobilized SiC NPs were also prepared. In this case, 200 μL of a Au@SiO_2-NH_2 particle dispersion (containing 1.4×10^{11} particles) was mixed with 3 μL of SiC NP dispersion (1 g L^{-1}) in water. The mixture was sonicated during 10 min. A summary of the elaboration conditions of NHs is given in Table 1.

Characterization methods

SEM images were obtained using an Inspect S50 microscope from FEI working at 10 kV. For SEM, samples were prepared by drop-casting of 2 μL of the Au@SiO_2 particles dispersion on a silicon wafer substrate. ImageJ 1.40 g software was used for image analysis.

TEM images were performed using a Topcon 002B microscope operating at 200 kV. For TEM studies, a drop of the diluted NH dispersion was deposited onto a carbon holey grid (ELOISE SARL).

UV–Visible absorption spectra were obtained on a SAFAS UV mc2 double-beam spectrophotometer by means of a microcuve of 1-mm length containing 5 μL of solution to analyze.

Zeta potential was evaluated by dynamic light scattering using a Zetasizer from Malvern Instruments.

Infra-red spectra were done in ATR mode using a Nicolet 6700 spectrometer from Thermo Scientific.

For the room temperature fluorescence spectra, excitation light was obtained from the triplet frequency ($\lambda_1 = 343$ nm) of a diode-pumped ytterbium femto-second laser or from an argon-ion laser with $\lambda_2 = 458$ nm or $\lambda_3 = 488$ nm. The solutions were poured into UV transparent quartz recipients. To evaluate the effect of the metal on the fluorescence of SiC NPs, diluted dispersion of SiC NPs in water was used as a reference. For the enhancement factor calculation, a reference was set to the same concentration initially added in the solution of NHs. The enhancement factor was calculated by the ratio between the fluorescence intensities of NHs and SiC references.

Results and discussion

Synthesis of Au@SiO_2 particles

The synthesis of Au@SiO_2 particles was performed following a reported two-step process with few modifications (Liz-Marzán et al. 1996). In the first step, a thin layer of silica (~2 nm) is formed around gold colloids in aqueous solution. The aim is to form a "vitreophilic" surface on Au colloids by replacing the initial sodium citrate surfactant by APTMS owing to the affinity of gold with amino groups. Then, TEOS, in the presence of a basic reagent, is added to grow a thicker silica shell. This method allows a good control over the size and morphology of silica beads depending on the amount of TEOS, solvent, and basic reagent. The size distribution of Au@SiO_2 particles was first controlled by SEM. The images show the formation of homogeneous size distribution (Fig. 2). The thickness of the silica shell can be varied from 25 to 80 nm depending on the amount of TEOS in the synthesis process with the same size homogeneity. Absorption spectroscopy of Au@SiO_2 particles in water solution was used to check the dependence of the plasmon band position of gold as a function of silica shell thickness (Fig. 3). The plasmon resonance of Au and Au@SiO_2 particles locates in the region of

Table 1 Elaboration conditions of NHs

Sample name	Silica shell thickness (nm)	Immobilization method	Volume of 1 g L^{-1} SiC NPs dispersion (μL)
C25-3	25	Covalent bonding	3
C40-3	40	Covalent bonding	3
C80-3	80	Covalent bonding	3
E25-3 (negative control)	25	Electrostatic bonding	3

In the sample name, the first letter stands for the immobilization methods (*C* covalent, *E* electrostatic), the first number for the silica shell thickness in nm, and the final number to the volume of SiC NPs dispersion (1 g L^{-1}) added for coupling

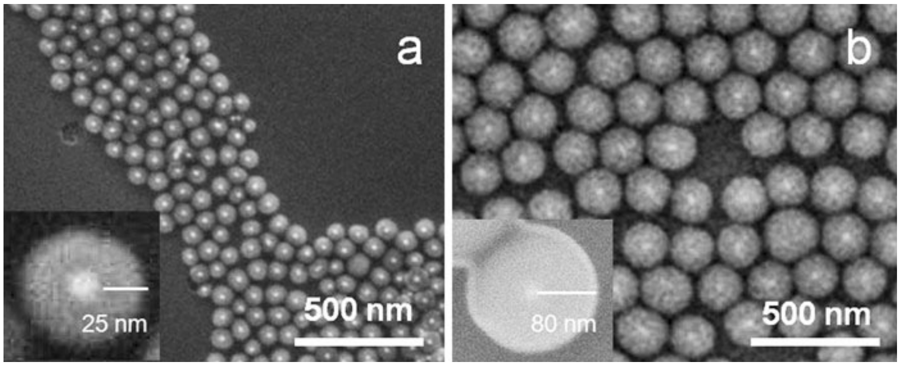

Fig. 2 SEM image of 20 nm-gold colloids coated with a silica shell of different thickness: **a** Au@SiO_2-25 nm and **b** Au@SiO_2-80 nm. The inserts show high magnification images of a single particle

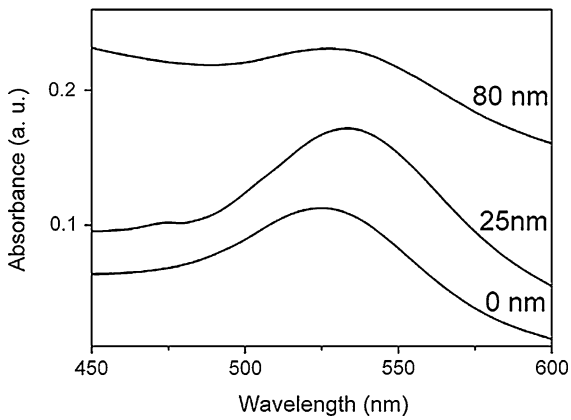

Fig. 3 Absorption spectra of Au@SiO_2 particles with different thickness of silica shell

520–530 nm even if a weak shift is observed depending on the silica shell thickness. As the thickness of silica shell increases from 0 to 25 nm, the intensity of absorbance is increased and a slight red-shift of the absorption maximum is observed due to the increase of the local refractive index around the Au colloids. For silica shell thicker than 40 nm, scattering is important, and thus a stronger absorbance is observed at shorter wavelengths, resulting in a weak blue-shift and a lower intensity of the plasmon band (Liz-Marzán et al. 1996).

Synthesis of NHs: covalent grafting of SiC NPs on Au@SiO_2 particles

Several pending chemical groups are present at the surface of SiC NPs—silanols, carboxylic acids, and carboxylates—making their surface negatively charged (Alekseev et al. 2007; Zakharko et al. 2010). These groups can be exploited for their covalent immobilization on Au@SiO_2. For instance, carboxylic functions can be reacted with amine leading to the formation of an amide bond. Thus, Au@SiO_2 surface was functionalized with amino groups. The density of amino groups on the silica surface was evaluated to 1.05×10^{14} NH_2/cm^2 by a colorimetric titration using Brilliant Coomassie Blue (Coussot et al. 2009). In addition, the mean Zeta potential of Au@SiO_2 particles evolved from -23 to -11 mV after amino functionalization. However, the Zeta potential remained negative probably because unreacted silanol functions remain at the surface of silica, indicating that the silica surface is not totally passivated.

Amino-functionalized Au@SiO_2 particles were covalently bonded to SiC NPs via the formation of an amide bond Au@SiO_2-NH-CO-SiC using an activated ester of SiC carboxylic pending groups. A negative control (E25-3) consisting of unactivated SiC NPs was also prepared. In this case, no amide bond should be formed. The elaboration of this negative control was to insure that (i) SiC immobilization was due to the formation of an amide bond (not to physical adsorption), (ii) the chemical signature (IR spectra) was not the result of potential surface contaminations resulting from the chemical reactions, and (iii) fluorescence enhancement was not the result of potential surface contaminations resulting from the chemical reactions. The infrared spectrum of C25-3 NHs (Fig. 4a) was compared to one of the negative control E25-3 (Fig. 4b).

In the case of E25-3, characteristic peaks at 1725, 1600, and 1540–1510 cm^{-1} were observed and correspond to the C=O (free COOH) stretching vibration,

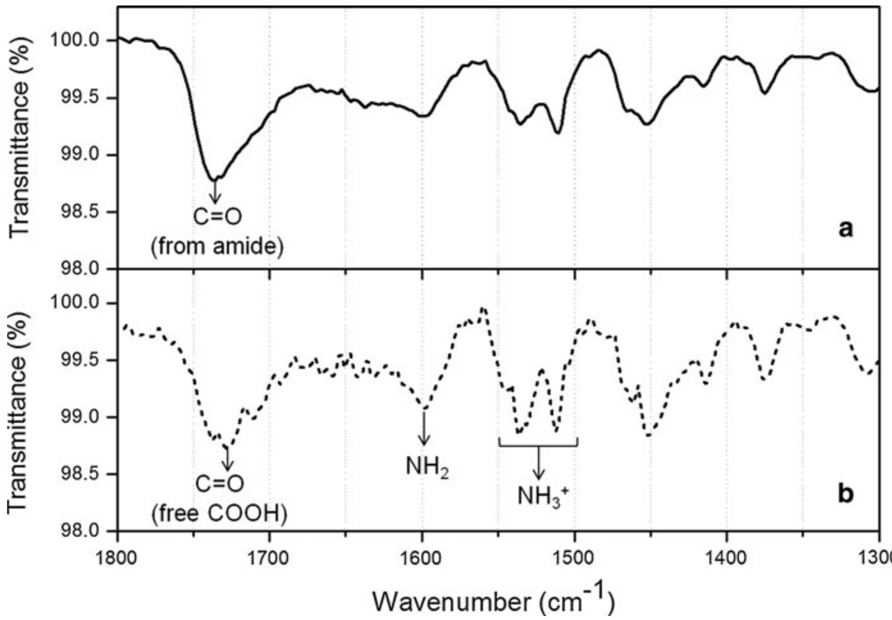

Fig. 4 IR spectra of **a** C25-3 NHs **b** E25-3 negative control

primary amine groups, and ammonium groups bending vibrations, respectively. In the case of covalently immobilized SiC NPs (C25-3), the carboxylic acid peak was shifted at 1,735 cm^{-1}, which corresponds to C=O groups implicated in the covalent bond. The peaks related to primary amines and ammonium were less intense (compared to the peak of C=O) in the NHs prepared by covalent bonding, proving that a majority of amino groups were involved in an amide bond.

The immobilization of SiC NPs onto silica was then controlled by TEM (Fig. 5). TEM images show that the immobilized SiC NPs formed a submonolayer on silica surfaces for both negative control (Fig. 5a) and covalent bonding (Fig. 5b). In this layer, SiC NPs were separated from each other by approximately an average distance higher than 6 nm. This result is not surprising because after calculation, the volume of SiC NP dispersion was chosen to be sure that all the SiC NPs added will be immobilized onto silica. In this case, an incomplete monolayer is obtained as shown in Fig. 5b.

For negative control E25-3, several isolated SiC NPs can be found (encircled in Fig. 5a). Isolated SiC NPs were never observed (Fig. 5b) after ester activation of carboxylic function illustrating the stability of the covalent bonding (vs. the negative control).

The fluorescence properties of the E25-3 and C25-3 were then compared (Fig. 6). All fluorescence spectra exhibited intense Raman peaks around 585 nm due to water or ethanol/water dispersant (Burikov et al. 2010). The broad band at lower intensity which is located between 550 and 750 nm corresponds to the fluorescence signal of SiC NPs and NHs when excitation wavelength is 488 nm. To extract the enhancement factor, the spectra were extrapolated to eliminate the Raman peaks signal (dashed lines on Fig. 6a, b). This factor was determined by the ratio of the NHs over the SiC NPs' reference intensities. For the negative control (E25-3 NHs, Fig. 6a), a weak enhancement of 1.3 (at $\lambda_{em} = 582$ nm) was obtained and the shape of emission spectra was unchanged, while a strong enhancement (3.2 at $\lambda_{em} = 582$ nm) and a blue-shift of the spectrum was observed for C25-3 NHs (Fig. 6b). The weak enhancement obtained for electrostatic bonding can be attributed to the unstable immobilization of SiC NPs as shown on TEM image (Fig. 5a). In the case of the spectral reshaping observed for C25-3, our hypothesis is that the blue-shift can be due to strong surface chemistry modification of SiC NPs when they are covalently bonded to silica. Indeed, as previously described (Zakharko et al. 2010), chemical environment has a high influence on SiC NPs' fluorescence properties. Changing the dispersant, emission band can be shifted to hundreds of nanometers. Thus, the higher the dielectric constant is the thinner and more blue-shifted the corresponding fluorescence emission peak will be. It was also recently shown that SiC NPs embedded inside silica

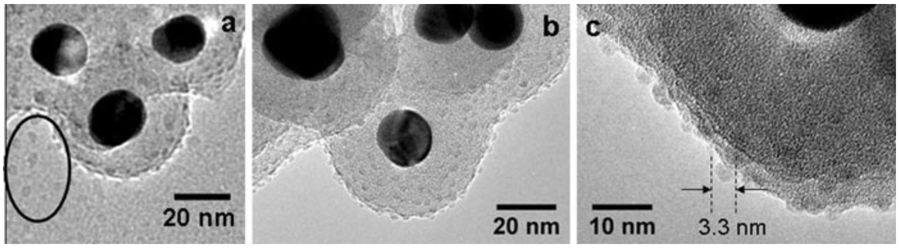

Fig. 5 TEM image of E25-3 (**a**), C25-3 (**b**) and C25-3 at higher magnification

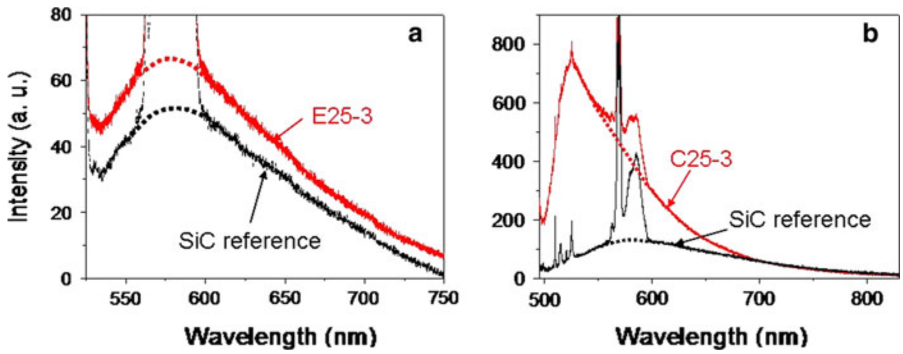

Fig. 6 Fluorescence spectra of E25-3 (**a**) and C25-3 (**b**) NHs compared to reference sample at excitation wavelength of 488 nm

spheres can exhibit an intense blue-light emission (Dai et al. 2011). To confirm this hypothesis, a reference sample involving silica particles without a gold core were prepared according to Stöber method (Stöber et al. 1968). SiC NPs were immobilized covalently with the same procedure as the one used for NHs. The SiC to silica particles ratio was the same as the one used for C25-3 NHs. The fluorescence spectrum of this SiO_2–SiC reference sample was compared to the fluorescence spectrum of SiC reference sample with the same concentration of SiC NPs (Fig. 7). The first remark is that the fluorescence intensity of SiC NP reference sample is quite the same as the fluorescence intensity of SiO_2–SiC reference sample, which proves that silica does not induce fluorescence enhancement. Second, the emission spectrum of SiO_2–SiC has a weak band at 523 nm, which can be attributed to the surface modification of SiC NPs when they are covalently linked to silica. This confirms our previous hypothesis.

Influence of silica shell thickness

The influence of silica thickness was then studied for NHs. The result obtained for C25-3 NHs (25 nm shell) presented in Fig. 6b was compared to two other silica shell thicknesses: 40 nm (C40-3) and 80 nm (C80-3). The fluorescence spectra are presented in Fig. 8 and enhancement factors obtained are summarized in Table 2.

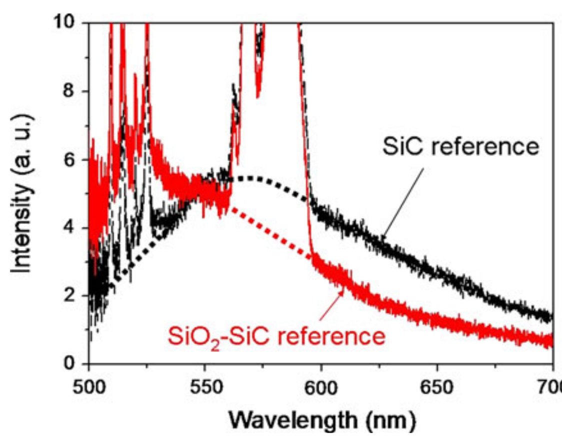

Fig. 7 Fluorescence spectra of reference samples: only SiC NPs and SiO_2-SiC NPs at excitation wavelength of 488 nm

As shown in Fig. 8 and Table 2, enhancement factor decreases when silica shell thickness increases. This result is consistent with previous work (Deng

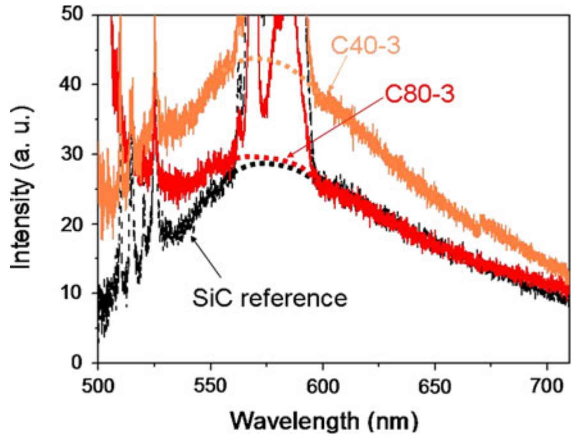

Fig. 8 Fluorescence spectra of C40-3 and C80-3 NHs compared to reference sample at excitation wavelength of 488 nm

Table 2 Enhancement factors obtained for NHs prepared by covalent bonding of SiC NPs at excitation wavelength of 488 nm. Measurements were done for different thickness of silica (25, 40, and 80 nm) and at two different wavelengths of fluorescence emission: $\lambda_{em} = 523$ nm and $\lambda_{em} = 582$ nm

Sample name	Enhancement factor	
	At $\lambda_{em} = 523$ nm	At $\lambda_{em} = 582$ nm
C25-3	12.5	3.2
C40-3	1.9	1.5
C80-3	1.7	1.0

et al. 2011). A high enhancement factor was measured for covalent NHs with 25-nm shell, while weak enhancement factor close to 1 was measured for 80-nm shell. Thus, it seems that for 80-nm thickness, the influence of gold plasmon on SiC NPs is negligible. This is confirmed by the weak intensity of gold plasmon band observed in Fig. 3. An evolution of the fluorescence spectra can also be observed with increasing thickness; in particular, in the region between 500 and 550 nm. Indeed, we have already explained the presence of an intense emission at 523 nm in the case of C25-3 NHs (Fig. 6b), which was attributed to to fluorescence enhancement and to SiC surface modification. In Fig. 8, this band is present, but with very weak intensity, for C40-3 NHs, while it is totally absent for C80-3 NHs. For C80-3 NHs; the measured intensity between 500 and 525 nm is only due to scattering of the excitation light by this large Au@SiO_2 particles (180 nm of diameter).

Influence of excitation wavelength

The influence of different excitation wavelengths (343, 458, and 488 nm) was then investigated on (Au@SiO_2)SiC NHs elaborated by covalent bonding and with a silica thickness of 25 nm. Spectra are presented in Fig. 9. The first observation is that the shape of the spectra strongly depends on the excitation wavelength, both for SiC NPs and NHs. When excitation wavelength was located in the UV region (343 nm, Fig. 9a), the fluorescence emission spectra exhibited two bands, the first one at 440 nm and the second one at 530 nm, for both NPs and NHs. The presence of these two bands was already evidenced (Wu et al. 2009). The first one is due to quantum-confined electron hole transition in the smallest NP core, while the second is most probably due to surface defect recombination. Obviously, when excitation wavelength was above 440 nm (458 nm, Fig. 9b), only the green band (540 nm) was observed for both NPs and NHs. The two sharp peaks observed at 529 and 543 nm corresponded to the Raman peak of the water/ethanol mixture (Burikov et al. 2010). The emission band of SiC NPs was centered at 550 nm, while the emission band of C25-3 NHs was centered at 540 nm. Finally, when excitation wavelength was at 488 nm (Fig. 9c), the two Raman peaks were shifted, respectively, to 570 and 585 nm. At this excitation wavelength, SiC NPs exhibited a broad emission band centered at 582 nm, while NHs had a narrower emission peak around 523 nm.

When excitation wavelength was set at 343 nm, the enhancement factor was below 1 for both emission wavelengths illustrating a strong quenching (Fig. 9d). At 458 nm, a weak enhancement was observed. Finally, at an excitation wavelength of 488 nm, enhancement factors of 3.2 and 12.5 were observed at 523 and 582 nm, respectively. According to these results, it seems that SiC NPs fluorescence on NHs is enhanced when the excitation wavelength is close to the Au colloids' absorption/plasmon band. Indeed, it has been reported that the excitation of gold-localized surface plasmon resonance modes results in the confinement of electromagnetic waves in regions near the metal surface. In the presence of a fluorophore, the resulting electromagnetic enhancement can induce a strong increase of fluorescence emission (Lakowicz 2001; Shimizu et al. 2002) or fluorescence resonance energy transfer (FRET). In the latter case, quenching of

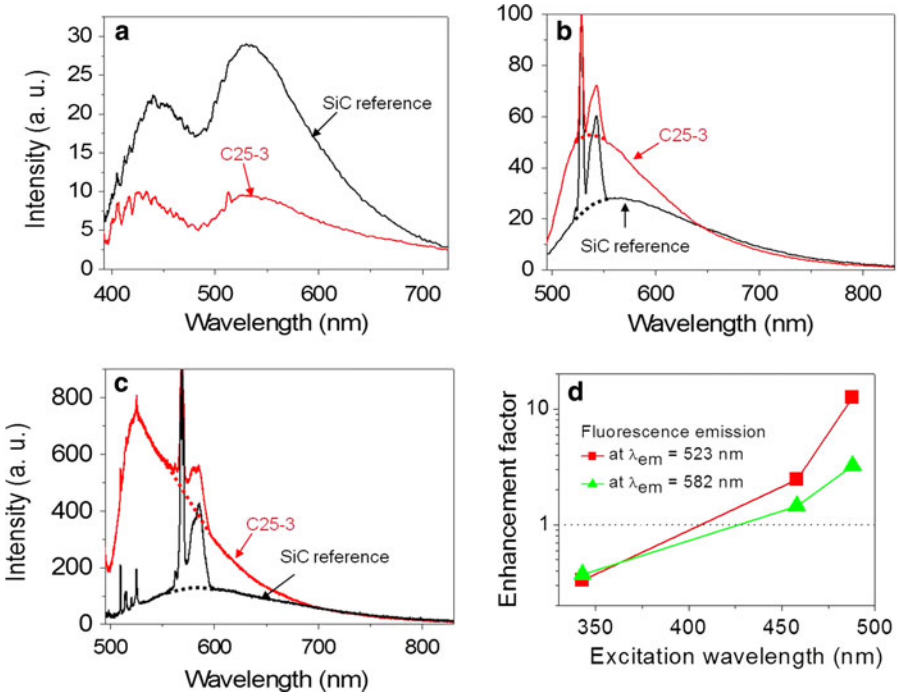

Fig. 9 Fluorescence spectra of C25-3 NHs compared to SiC reference samples for different excitation wavelengths: 343 nm (**a**), 458 nm (**b**) and 488 nm (**c**). Enhancement factor calculation for two different emission wavelengths (**d**): $\lambda_{em} = 523$ nm (*squares*) and $\lambda_{em} = 582$ nm (*triangles*)

the fluorescence is observed (Goulet and Aroca 2005). In our case, when the excitation wavelength is at 343 nm, the absorption/plasmon band of gold colloids totally overlaps the fluorescence band of SiC NPs (as shown in supporting information). This is typically the situation where fluorescence quenching is observed due to energy transfer. Thus, the plasmon of Au@SiO_2 may "re-absorb" the fluorescence of SiC NPs. This is not the case for excitation at 458 and 488 nm for which plasmon is more efficiently excited by the laser. That is why, for these excitation wavelengths, enhancement can be observed. A similar behavior was recently observed for CdSe/ZnS—DNA linked—Au nanoparticle heterodimers (Maye et al. 2010). Therefore, fluorescence properties of NHs have to be studied at 488 nm, as close as possible to the Au@SiO_2 plasmon band.

Conclusion

In conclusion, we have elaborated new (Au@SiO_2)SiC NHs with controlled silica thickness and covalent immobilization of SiC NPs at the surface of silica. These NHs show interesting fluorescent properties which can be plasmon controlled. For these NHs, a blue-shift of fluorescence appears compared to the initial emission of SiC NPs. This behavior was attributed to the strong surface modification of SiC NPs when they are covalently bonded to silica. We have shown that enhancement/quenching properties are influenced by excitation wavelength, stability of SiC immobilization onto silica, and silica shell thickness. Ideally, to obtain highest enhancement factors (i) the excitation must be performed as close as possible to the gold plasmon band, (ii) the immobilization of SiC NPs must be covalent to avoid isolated NPs in the solution, and (iii) the silica shell thickness must be sufficiently thin so that the electric field due to plasmon may have an influence on SiC NPs. We are now investigating the use of these NHs as fluorescent labels for cell imaging.

Acknowledgements We are indebted to the Chinese Scholarship Council for the financial support of N. Sui. We also thank Ecole Centrale de Lyon and INSA Lyon for the salary of Dr. S. Alekseev as an invited professor. Dr. N. Blanchard is thanked for support with TEM experiments and Dr. V. Dugas for the help with Coomassie Blue titration.

References

Alekseev S, Botsoa J, Zaitsev VN, Barbier D (2007) Fourier transform infrared spectroscopy and temperature-programmed desorption mass spectrometry study of surface chemistry of porous 6H-SiC. Chem Mater 19:2189–2194

Botsoa J (2008) Synthèse de nanostructures de carbure de silicium et étude de leurs propriétés optiques. Ph.D. Thesis, Institut National des Sciences Appliquées de Lyon

Botsoa J, Lysenko V, Géloën A, Marty O, Bluet JM, Guillot G (2008) Application of 3C-SiC quantum dots for living cell imaging. Appl Phys Lett 92:173902

Burikov S, Dolenko T, Patsaeva S, Starokurov Y, Yuzhakov V (2010) Raman and IR spectroscopy research on hydrogen bonding in water-ethanol systems. Mol Phys 108:2427–2436

Coussot G, Nicol E, Commeyras A, Desvignes I, Pascal R, Vandenabeele-Trambouze O (2009) Colorimetric quantification of amino groups in linear and dendritic structures. Polym Int 58:511–518

Dai D, Fan J, Zhang N (2011) Synthesis and luminescence properties of silica-coated cubic silicon carbide nanocrystal composites. Micro Nano Lett 6:878–880

Deng W, Jin D, Drozdowicz-Tomsia K, Yuan J, Wu J, Goldys EM (2011) Ultrabright Eu-doped plasmonic Ag@SiO_2 nanostructures: time-gated bioprobes with single particle sensitivity and negligible background. Adv Mater 23:4649–4654

Fan J, Li H, Jiang J, So LKY, Lam YW, Chu PK (2008) 3C-SiC nanocrystals as fluorescent biological labels. Small 4: 1058–1062

Goulet PJG, Aroca RF (2005) Surface-enhancement of fluorescence near noble metal nanostructures. In: Lakowicz JR, Geddes CD (eds) Radiative decay engineering. Topics in fluorescence spectroscopy, vol 8. Springer, New York, pp 230–231

Lakowicz JR (2001) Radiative decay engineering: biophysical and biomedical applications. Anal Biochem 298:1–24

Lakowicz JR (2006) Plasmonics in biology and plasmon-controlled fluorescence. Plasmonics 1:5–33

Liu N, Prall BS, Klimov VI (2006) Hybrid gold/silica/nanocrystal-quantum-dot superstructures: synthesis and analysis of semiconductor-metal interactions. J Am Chem Soc 128:15362–15363

Liz-Marzán LM, Giersig M, Mulvaney P (1996) Synthesis of nanosized gold-silica core-shell particles. Langmuir 12: 4329–4335

Maye MM, Gang O, Cotlet M (2010) Photoluminescence enhancement in CdSe/ZnS–DNA linked–Au nanoparticle heterodimers probed by single molecule spectroscopy. Chem Commun 46:6111–6113

Mélinon P, Masenelli B, Tournus F, Perez A (2007) Playing with carbon and silicon at the nanoscale. Nat Mater 6:479–490

Ming T, Zhao L, Yang Z, Chen H, Sun L, Wang J, Yan C (2009) Strong polarization dependence of plasmon-enhanced fluorescence on single gold nanorods. Nano Lett 9:3896–3903

Resch-Genger U, Grabolle M, Cavaliere-Jaricot S, Nitschke R, Nann T (2008) Quantum dots versus organic dyes as fluorescent labels. Nat Methods 5:763–775

Shimizu KT, Woo WK, Fisher BR, Eisler HJ, Bawendi MG (2002) Surface-enhanced emission from single semiconductor nanocrystals. Phys Rev Lett 89:117401

Stöber W, Fink A, Bohn E (1968) Controlled growth of monodisperse silica spheres in the micron size range. J Colloid Interf Sci 26:62–69

Tovmachenko OG, Graf C, VandenHeuvel DJ, VanBlaaderen A, Gerritsen HC (2006) Fluorescence enhancement by metal-core/silica-shell nanoparticles. Adv Mater 18:91

VanBlaaderen A, Vrij A (1993) Synthesis and characterization of monodisperse colloidal organo-silica spheres. J Colloid Interf Sci 156:1–18

Westcott SL, Oldenburg SJ, Lee TR, Halas NJ (1998) Formation and adsorption of clusters of gold nanoparticles onto functionalized silica nanoparticle surfaces. Langmuir 14:5396–5401

Wu XL, Xiong SJ, Zhu J, Wang J, Shen JC, Chu PK (2009) Identification of surface structures on 3C-SiC nanocrystals with hydrogen and hydroxyl bonding by photoluminescence. Nano Lett 9:4053–4060

Zakharko Y, Botsoa J, Alekseev S, Lysenko V, Bluet JM, Marty O, Skryshevsky VA, Guillot G (2010) Influence of the interfacial chemical environment on the luminescence of 3C-SiC nanoparticles. J Appl Phys 107:013503

Zhang F, Braun GB, Shi Y, Sun X, Reich NO, Zhao D, Stucky G (2010) Fabrication of Ag@SiO_2@Y_2O_3:Er nanostructures for bioimaging: tuning of the upconversion fluorescence with silver nanoparticles. J Am Chem Soc 132:2850–2851

Zheng Q, Zhang Y, Liu X, Tu L, Wang Y, Kong X, Zhang H (2010) Au/SiO_2 core/shell nanoparticles enhancing fluorescence energy transfer efficiency in solution. Chem Commun 46:6479–64781